# Spin-valley-dependent transport and giant tunneling magnetoresistance in silicene with periodic electromagnetic modulations*

Yi-Man Liu(刘一曼)[1], Huai-Hua Shao(邵怀华)[2], Guang-Hui Zhou(周光辉)[3], Hong-Guang Piao(朴红光)[1], Li-Qing Pan(潘礼庆)[1], and Min Liu(刘敏)[1,†]

[1] *College of Science, China Three Gorges University, Yichang* 443002, *China*
[2] *School of Electrical Engineering, Liupanshui Normal University, Liupanshui* 553004, *China*
[3] *Department of Physics and Key Laboratory for Low-Dimensional Structures and Quantum Manipulation (Ministry of Education), Hunan Normal University, Changsha* 410081, *China*

(Received 23 July 2017; revised manuscript received 4 September 2017; published online 20 November 2017)

The transport property of electrons tunneling through arrays of magnetic and electric barriers is studied in silicene. In the tunneling transmission spectrum, the spin-valley-dependent filtered states can be achieved in an incident energy range which can be controlled by the electric gate voltage. For the parallel magnetization configuration, the transmission is asymmetric with respect to the incident angle $\theta$, and electrons with a very large negative incident angle can always transmit in propagating modes for one of the spin-valley filtered states under a certain electromagnetic condition. But for the antiparallel configuration, the transmission is symmetric about $\theta$ and there is no such transmission channel. The difference of the transmission between the two configurations leads to a giant tunneling magnetoresistance (TMR) effect. The TMR can reach to 100% in a certain Fermi energy interval around the electrostatic potential. This energy interval can be adjusted significantly by the magnetic field and/or electric gate voltage. The results obtained may be useful for future valleytronic and spintronic applications, as well as magnetoresistance device based on silicene.

**Keywords:** silicene, quantum transport, electromagnetic superlattice, giant tunneling magnetoresistance effect

**PACS:** 73.23.–b, 73.63.–b, 73.43.Qt, 85.75.–d **DOI:** 10.1088/1674-1056/26/12/127303

## 1. Introduction

Silicene, a two-dimensional (2D) silicon[1] akin to graphene[2] but with slightly buckled honeycomb structure, has been successfully obtained experimentally[3,4] and attracted plenty of interests in theoretical research.[5–12] In silicene, the energy spectrum of carriers consists of two valleys labeled by two inequivalent points (referred to as $K$ and $K'$) at the edges of the hexagonal Brillouin zone (BZ). Each valley has a Dirac-like electron dispersion near the points where the electron and hole bands have a gap of 1.55 meV–7.9 meV caused by spin–orbit coupling (SOC).[5,6] This gap is much larger than graphene.[13] Moreover, the buckled structure provides us a method to tune the band gap easily via a perpendicular external electrical field.[8,14] Such a peculiar band structure of silicene makes experimentally accessible to quantum spin/valley Hall effect, quantum anomalous Hall effect, and spin/valley-polarized metal phases.[5–7,15–20] These effects make silicene a promising material for spin-tronic and valley-tronic applications.

In the presence of a perpendicular uniform magnetic field, the spin- and valley-polarized levels due to the SOC and electric field gating of silicene result in a polarized magneto-optical conductivity;[21] a uniform electric field modulation leads to valley polarized quantum Hall effect (VQHE)[22] and a periodic potential or electric field modulations can result in spin- and valley-resolved magnetotransports.[23] Beyond uniform magnetic field, the nonuniform magnetic fields can define various magnetic nanostructures ranging from magnetic barriers and wells[24,25] to magnetic dots and antidotes.[26] This provide another clue to the manipulation of electrons not only in graphene[27–29] and three-dimensional topological insulator surface,[30,31] but also in silicene.[32,33] In particular, the properties of Dirac electrons in graphene and the surface of topological insulator under a periodic magnetic confinement were discussed.[34,35] However, less attention has been paid to the effects of a periodic local magnetic field modulations on 2D Dirac quasiparticle in silicene.

In this paper, we study the electron tunneling through a silicene superlattice of magnetic and electric barriers, as shown in Fig. 1, where we consider the magnetic barriers with delta-function-shaped magnetic fields. This kind of magnetic field profiles can be created by depositing ferromagnetic metallic (FM) strips at equal spacing with the magnetization

*Project supported by the National Natural Science Foundation of China (Grant Nos. 11547249, 51501102, and 11647157) and the Science Foundation for Excellent Youth Doctors of Three Gorges University, China (Grant No. KJ2014B076).

†Corresponding author. E-mail: lmin@ctgu.edu.cn

© 2017 Chinese Physical Society and IOP Publishing Ltd 

parallel to the plane on top of the insulating layer, as proposed for in graphene,[29,34,36] thus forming a magnetic superlattice along $x$ axis. Using the scattering matrix method,[37–39] we investigate theoretically the transmission and conductance for periodic arrangements of magnetic barriers with parallel (P) and antiparallel (AP) magnetic field configurations. We should point out that the scattering between different valleys is unavoidable.[40] However, in the calculations, the intervalley scattering can be neglected because of a slight impact on the transport properties in our considered system.[41,42] We find that the tunneling transmission is asymmetric with respect to the in-plane momentum $k_y$ for P configuration but symmetric about $k_y$ for AP configuration. The interplay of massive electrons with spin–orbit coupling in silicene results in a spin-valley dependent gap. Thus, different spins and valleys arise different spin-valley dependent states. Therefore, whenever the perpendicular external electric field in FM regions are nonzero, there is a particular incident energy range where only one spin from one valley and opposite spin from the opposite valley are transmitted. The transmission feature depends on the spin-valley indices due to the coupling between valley and spin degrees of freedom. This spin-valley-dependent transport is found to be controllable by the electric gate voltage and magnetic field. Moreover, the difference of the transmission between the P and AP configurations leads to a giant tunneling magnetoresistance (TMR) effect. The TMR can be tuned significantly by the magnetic field and the height of electrostatic potential.

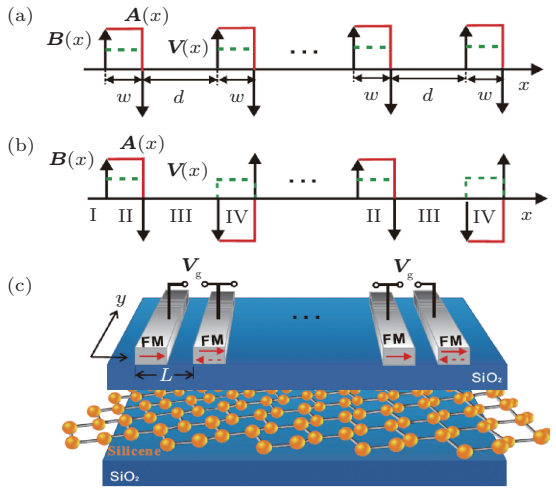



**Fig. 1.** (color online) (a) Simplified profiles of the magnetic barrier for the P alignment (spikelike lines), the corresponding vector potential $A_y(x)$ (red solid line), and the electrostatic potential $V(x)$ (green dashed line). (b) The same as in panel (a) but for the AP alignment. (c) The schematic illustration of the considered 2D electron system modulated by an array of FM stripes deposited on top of the silicene sheet. The red horizontal arrows denote the magnetization directions (along $x$ axis) of the strips that generate an array of delta-function-shaped magnetic barriers. The gate voltage $V_g$ applied on FM stripes provides a periodic array of electrostatic barriers.

The organization of the paper is as follows. In Section 2, we present and explain the model Hamiltonian, where the scattering matrix technique is adopted to calculate the transmission probability. In Section 3, we show contour plots of the tunneling transmission probability as a function of incident energy and angle for P and AP configurations. Moreover, we show the behavior of the charge conductances and TMR. Finally, in Section 4 we summarize the results.

## 2. Model and formalism

The low energy effective Hamiltonian around $K$ ($K'$) point in BZ for electrons in silicene under the modulation of inhomogeneous perpendicular magnetic field and electric field can be written as[5–7,21,23]

$$H_{\eta,\sigma} = v_{\rm F}(\pi_x\tau_x - \eta\pi_y\tau_y) - \eta\sigma\Delta_{\rm so}\tau_z + \Delta_z\tau_z + V\tau_0, \quad (1)$$

where $\eta = +/-1$ labels the $K/K'$ valley, $\sigma = +/-1$ donates spin-up ($\uparrow$)/spin-down ($\downarrow$), $\tau_i$ ($i = x,y,z$) are the Pauli matrices acting on pseudospin degree, $\tau_0$ is the unit matrix, the Fermi velocity $v_{\rm F} \approx 5\times10^5$ m/s, and the intrinsic SOC strength $\Delta_{\rm so} = 3.9$ meV,[6] $\boldsymbol{\pi} = \hbar\boldsymbol{k} + e\boldsymbol{A}$ is the 2D momentum in the Hamiltonian with wave vector $\boldsymbol{k}$ and magnetic vector potential $\boldsymbol{A}$.

In this work, we consider arrays of identical magnetic barriers with delta-function-shaped magnetic fields at the edges of the barriers as shown in Fig. 1. The magnetic field is perpendicular to the silicene sheet and can be given by

$$\boldsymbol{B}(x) = Bl_{B_0}\{[\delta(x-nL) - \delta(x-w-nL)] + \gamma[\delta(x-w-d-nL) - \delta(x-2w-d-nL)]\}\hat{z} \quad (2)$$

with $n = 0,2,4,6,\ldots,N-2$ ($N$ denotes the even number of FM stripes), the $\delta$-function $\delta(\cdot)$ and step-function $\theta(\cdot)$, $w$ the width of each FM stripe, $d$ the distance between adjacent FM stripes and the lattice constant $L = w+d$. Here, $B$ gives the strength of the local magnetic field, $l_B = \sqrt{\hbar/eB_0}$ is the magnetic length for an estimated magnetic field $B_0$. And $\gamma = \pm1$ represents the magnetization configuration corresponding to the P and AP configuration. We employ the Landau gauge for the vector potential $\boldsymbol{A} = [0, A_y(x), 0]$. The corresponding magnetic vector potential

$$A_y(x) = Bl_{B_0}\{[\theta(x-nL) - \theta(x-w-nL)] + \gamma[\theta(x-w-d-nL) - \theta(x-2w-d-nL)]\}. \quad (3)$$

Moreover, a tunable electrostatic barrier potential $V(x) = U_0[\theta(x-nL)\theta(w-x+nL) + \theta(x-w-d-nL)\theta(2w+d-x+nL)]$ is applied on silicene sheet with height $U_0 > 0$. The on-site potential difference between sublattice A and B is $\Delta_z(x) = \Delta_z[\theta(x-nL)\theta(w-x+nL) + \theta(x-w-d-nL)\theta(2w+d-x+nL)]$, where $\Delta_z = lE_z$ with the buckling distance $l = 0.46$ Å can be efficiently tuned by a local perpendicular electric field $E_z$ using a combination of top and bottom gates.[14,15]

For simplicity, we express all quantities in dimensionless units by introducing two characteristic parameters: the magnetic length $l_{B_0}$ and energy $E_0 = \hbar v_{\rm F}/l_{B_0}$. Taking a realistic value $B_0 = 0.1$ T, so the concerned parameters $l_{B_0} = 81$ nm and $E_0 = 4$ meV. In each specific region, the vector potential $A_y$ and electrostatic potential $V$ all are constant. Therefore the eigenequation of model Hamiltonian can be specifically rewritten as

$$\begin{pmatrix} -\eta\sigma\Delta_{\rm so}+\Delta_z+V-E & k_x+{\rm i}\eta(k_y+A_y) \\ k_x-{\rm i}\eta(k_y+A_y) & \eta\sigma\Delta_{\rm so}-\Delta_z+V-E \end{pmatrix}\begin{pmatrix}\phi_{\rm A}\\ \phi_{\rm B}\end{pmatrix}=0, \tag{4}$$

with $\phi_{A/B}$ being the wave function component. In the presence of an inhomogeneous perpendicular magnetic field, the Zeeman energy has been ignored due to a slight effect on the transmission at our considered magnetic field,[21] and the transverse wave vector $k_y$ is conserved because of the translational invariance in the $y$ direction. From Eq. (4), the eigenvalues in the normal and ferromagnetic silicene can be easily deduced and the wave functions in each region can be further determined. In the normal region I [see Figs. 1(a) and 1(b)], the wave function for a given incident energy $E$ can be written as

$$\psi_1 = a_1 {\rm e}^{{\rm i}k_x x}\begin{pmatrix}k_x+{\rm i}\eta k_y\\ E+\eta\sigma\Delta_{\rm so}\end{pmatrix}+b_1{\rm e}^{-{\rm i}k_x x}\begin{pmatrix}-k_x+{\rm i}\eta k_y\\ E+\eta\sigma\Delta_{\rm so}\end{pmatrix} \tag{5}$$

with $k_x=\sqrt{E^2-(\eta\sigma\Delta_{\rm so})^2-k_y^2}$. In the barrier region II, the wave function can be expressed as

$$\psi_2 = a_2 {\rm e}^{{\rm i}k'_x x}\begin{pmatrix}k'_x+{\rm i}\eta\beta_+\\ E_M\end{pmatrix}+b_2{\rm e}^{-{\rm i}k'_x x}\begin{pmatrix}-k'_x+{\rm i}\eta\beta_+\\ E_M\end{pmatrix}, \tag{6}$$

where $k'_x=\sqrt{(E-U_0)^2-(\Delta_z-\eta\sigma\Delta_{\rm so})^2-(k_y+A_y)^2}$, $E_M = E-U_0-\Delta_z+\eta\sigma\Delta_{\rm so}$, and $\beta_\pm = k_y\pm A_y$. We can obtain a similar corresponding wave function to Eq. (5) in each normal region (region III), and a similar case to Eq. (6) in each barrier region (region II/IV) for the magnetic barrier with P alignment. However, for the case of the magnetic barrier with AP alignment, in the barrier region IV with negative magnetic vector potential, the wave function should be expressed as

$$\psi_4 = a_4 {\rm e}^{{\rm i}k''_x x}\begin{pmatrix}k''_x+{\rm i}\eta\beta_-\\ E_M\end{pmatrix}+b_4{\rm e}^{-{\rm i}k''_x x}\begin{pmatrix}-k''_x+{\rm i}\eta\beta_-\\ E_M\end{pmatrix} \tag{7}$$

with $k''_x=\sqrt{(E-U_0)^2-(\Delta_z-\eta\sigma\Delta_{\rm so})^2-(k_y-A_y)^2}$. $a_j$ and $b_j$ are the coefficients of the forward and the backward states in the $j$-th ($j=1,2,3,\ldots,2N+1$) region, respectively. The matrix relationship between the wave function coefficients can be expressed as

$$\begin{pmatrix}a_j\\ b_j\end{pmatrix}=M(j)\begin{pmatrix}a_{j+1}\\ b_{j+1}\end{pmatrix}, \tag{8}$$

where the explicit expressions of the transfer matrix $M(j)$ can be calculated by matching the continuity conditions for the wave functions at boundaries between different regions, i.e., $\psi_j(x_j)=\psi_{j+1}(x_j)$. Here $x_j$ is the $x$-coordinate for the boundary between regions $j$ and $j+1$. The full transfer matrix $M$ can be obtained from matrix multiplication of the individual matrices connecting adjacent regions, namely, $M = M(1)M(2)\ldots M(j)\ldots M(2N)$. In contrast to the transfer matrix method, scattering matrix method has the advantage of being stable for quantum systems with periodic potential modulations.[37,38] Therefore, we adopt the scattering matrix method to calculate the transmission probability. For a multilayer structure, the coefficients $a_j$ and $b_1$ of the outgoing states are related to the coefficients $a_1$ and $b_j$ of the incoming states via the scattering matrix $S(1,j)$:

$$\begin{pmatrix}a_j\\ b_1\end{pmatrix}=S(1,j)\begin{pmatrix}a_1\\ b_j\end{pmatrix}, \tag{9}$$

The coefficients $a_j$ and $b_j$ can be eliminated from Eqs. (8) and (9) to give the new scattering matrix $S(1,j+1)$:

$$\begin{pmatrix}a_{j+1}\\ b_1\end{pmatrix}=S(1,j+1)\begin{pmatrix}a_1\\ b_{j+1}\end{pmatrix}. \tag{10}$$

For a detailed derivation and explicit expressions of $S(1,j+1)$, we refer to Ref. [39]. Therefore, starting with the unit matrix $S(1,1)$, $S(1,2N+1)$ can be calculated through an iterative procedure:

$$\begin{pmatrix}a_{2N+1}\\ b_1\end{pmatrix}=S(1,2N+1)\begin{pmatrix}a_1\\ b_{2N+1}\end{pmatrix}=\begin{pmatrix}S_{11} & S_{12}\\ S_{21} & S_{22}\end{pmatrix}\begin{pmatrix}a_1\\ b_{2N+1}\end{pmatrix}. \tag{11}$$

In the last region $2N+1$, there is no backward states, $b_{2N+1}=0$. Therefore, the transmission probability

$$T_{\eta\sigma}(E,k_y)=\left|t_{\eta\sigma}(E,k_y)\right|^2=\left|a_{2N+1}/a_1\right|^2=\left|S_{11}\right|^2. \tag{12}$$

For the P/AP configuration, the ballistic conductance at zero temperature can be calculated from the Landauer–Büttiker formalism[43]

$$G_{\eta\sigma}=G_0\int_{-\pi/2}^{\pi/2}T_{\eta\sigma}(E_{\rm F},k_{\rm F}\sin\theta)\cos\theta\,{\rm d}\theta, \tag{13}$$

where $G_0={\rm e}^2L_yk_F/2\pi h$ is taken as the conductance unit with $k_{\rm F}=\sqrt{E_{\rm F}^2-\Delta_{\rm so}^2}$, $E_{\rm F}$ is the Fermi energy and $\theta$ is the incident angle, $L_y$ is the sample size along the $y$ direction which is much larger than $w$ and $d$.

## 3. Results and discussions

In what follows, to obtain the tunneling transmission features for the magnetic superlattice with P and AP configurations, we show contour plots of the transmission probability $T_{\eta\sigma}$ as a function of incident energy and angle in Fig. 2 (P alignment) and Fig. 3 (AP alignment) for different $\Delta_z$ and $U_0$. Furthermore, we show the behavior of the total charge conductances and the TMR in Fig. 4. In our calculations, we choose the magnetic barrier ($B = 1$) with a fixed width $w = 0.5$ and the smallest distance between two barriers $d = 2$. For larger $d$, the transmission exhibits more significant oscillation, but the qualitative behavior of all the transmission, conductances and TMR remain similar to our case.

We focus on the spin-valley transport in a bulk silicene. Obviously, for the bulk charge carriers, a common feature of all the cases depicted in Figs. 2 and 3 is that transmission is totally forbidden for the low-energy regime $E < \Delta_{so}$ regardless of the electrostatic potential $U_0$ and on-site potential difference $\Delta_z$. This is because in this regime the Fermi level is located inside the band gap near $K$ and $K'$ points in the incoming region (normal region I). We find that the transmissions for $\eta\sigma = 1$ states and $\eta\sigma = -1$ states are identical whenever $\Delta_z = 0$. Moreover, the plot of $T_{K\uparrow}$ is identical to $T_{K'\downarrow}$ ($\eta\sigma = 1$) and the plot of $T_{K\downarrow}$ is identical to $T_{K'\uparrow}$ ($\eta\sigma = -1$) for any case in our considered system.

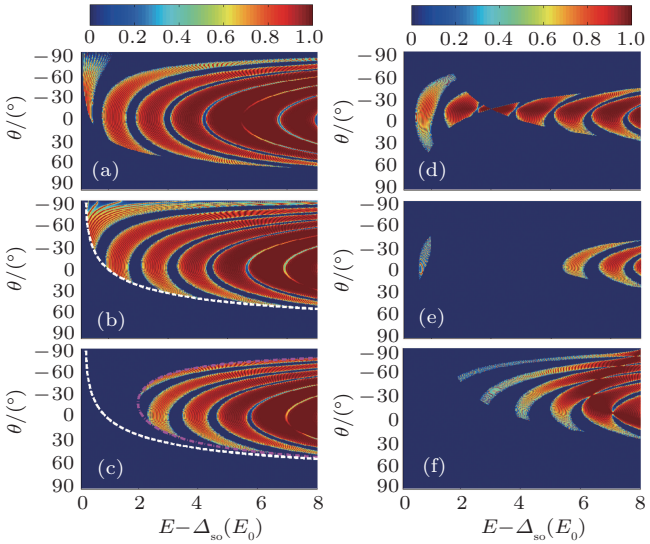



**Fig. 2.** (color online) The contour plot of the transmission probability $T_{\eta\sigma}$ as a function of the incident angle and incident energy for the parallel alignment with a fixed barrier width $w = 0.5$, distance $d = 2$, and magnetic field $B = 1$, (a) $T_{K\uparrow/K'\downarrow/K\downarrow/K'\uparrow}$, $\Delta_z = U_0 = 0$; $\Delta_z = \Delta_{so}$ for panels (b)–(f), (b) $T_{K\uparrow/K'\downarrow}$, $U_0 = 1$; (c) $T_{K\downarrow/K'\uparrow}$, $U_0 = 1$; (d) $T_{K\uparrow/K'\downarrow}$, $U_0 = 4$; (e) $T_{K\downarrow/K'\uparrow}$, $U_0 = 4$; (f) the same as panel (b) but for $B = 4$. The magnetic unit $B_0 = 0.1$ T, the energy unit is $E_0 = 4$ meV, and the length unit is $l_B = 81$ nm. The number of FM stripes is $N = 40$.

First we consider the tunneling process through the delta-function-shaped magnetic barriers with P configuration. In Fig. 2(a), the case of $\Delta_z = 0$ and $U_0 = 0$, we can see that the transmission is asymmetric with respect to the incident angle $\theta$ because of the present of magnetic field. The magnetic vector potential $A_y = B$ for our case, and the longitudinal momentum in the barrier region is given by $k'_x = \sqrt{E^2 - \Delta_{so}^2 - (k_y + B)^2}$ which is more likely to be imaginary with $k_y > 0$. As a result, electrons with positive incident angles are more likely to transmit through evanescent modes, and a transmission is usually allowable for a negative incident angle $\theta$. When the external electric fields $\Delta_z \neq 0$ are applied in the same region as the magnetic barriers and $U_0 = 0$, we can infer that the transmission is also in a wide region of $\theta$ but is forbidden in the energy range $E < \max(\Delta_z - \eta\sigma\Delta_{so}, \Delta_{so})$.

In Figs. 2(b)–2(f), we show the effect of a combined on-site potential difference and electrostatic potential on the transmission. For the case $\Delta_z = \Delta_{so}$ and $U_0 = E_0$, it is interesting to find that the transmission is remarkable in all the region with negative incident angles for $\eta\sigma = 1$ states [See Fig.2(b)]. The transmission is forbidden outside the transmission window delineated by the dashed white line which is the boundary of the total reflection region ($T = 0$) and is determined by the critical condition $(k_y + B)^2 = (E - E_0)^2$. The transmission can occur with the incident energy above the critical value. However, in this case, the transmission in the region with large negative incident angles for $\eta\sigma = -1$ states is suppressed as shown in Fig.2(c). This leads to the appearance of a wide region, between the dash-dotted purple line and white line in this figure, where only $\eta\sigma = 1$ states are not suppressed. In other words, in this region only spin up states from the $K$ valley and spin down states from the $K'$ valley are transmitted. When the electrostatic potential increases to $U_0 > B$ (in dimensionless units), we find that the transmission is heavily suppressed in an energy interval around the electrostatic potential [See Fig. 2(d) and (e)]. This can be understood as follows. According to the relationship $k_x'^2 + (k_y + B)^2 = (E - U_0)^2 - (\Delta_z - \eta\sigma\Delta_{so})^2$, the wave vector $k'_x$ in the barrier tends to be imaginary when $(k_y + B)^2 > (E - U_0)^2 - (\Delta_z - \eta\sigma\Delta_{so})^2$. Obviously, this inequality is true for any value of $k_y$ as the incident energy becomes closer to the electrostatic potential. Therefore, the evanescent modes decay rapidly in the barrier regions and lead to the suppression of transmission. There is a broad energy interval $-(\Delta_z + \Delta_{so}) + U_0 < E < (\Delta_z + \Delta_{so}) + U_0$ where the reflection is complete in the whole $\theta$ region for $\eta\sigma = -1$ states. By comparing Figs. 2(b) with 2(f), we can see that the evanescent modes with large imaginary wave vectors in barriers reduce the transmission probability more significantly with the increase of magnetic barrier height, thus more transmission peaks disappear in the region with positive incident angles and low incident energies. Furthermore, if we increase the magnetic barrier and electric potential barrier height simultaneously, as well as $B = U_0$, electrons can always transmit via propagating states in the superlattice region in a large negative angle $\theta$ closing to $-90°$ for $\eta\sigma = 1$ states except the low-energy regime [see Fig. 2(b) ].

Next we discuss the transmission characteristics for the AP configuration, which is shown in Figs. 3(a)–3(f). For this configuration, the transmission becomes symmetric with respect to $\theta$. From Fig. 1(b), we know that the magnetic vector potential $A_y(x)$ is antisymmetric about the center ($x = 0$) of the whole structure. However, the system has a symmetry associated with the operation $U = \hat{T}\hat{R}_x\hat{\sigma}_y$,[29] where $\hat{T}$ is the time-reversal operator, $\hat{R}_x$ is the reflection operator about the center of the superlattice, and $\hat{\sigma}_y$ is one of the Pauli matrices. Under this unitary transformation, we have $H'_{\eta,\sigma} = UH_{\eta,\sigma}[k_x, k_y + A_y(-x), \Delta_z(-x), U(-x)]U^{-1} = k_x\tau_x - \eta[k_y + A_y(-x)]\tau_y - \eta\sigma\Delta_{so}\tau_z + \Delta_z(-x)\tau_z + V(-x)\tau_0$. It implies that in the case of AP configuration, $A_y(-x) = -A_y(x)$, $\Delta_z(-x) = \Delta_z(x)$, $V(-x) = V(x)$, $H'_{\eta,\sigma}(-k_y) = H^*_{\eta,\sigma}(k_y)$, which means that the transmission spectrum is symmetric about $k_y = 0$, as shown in Fig. 3.

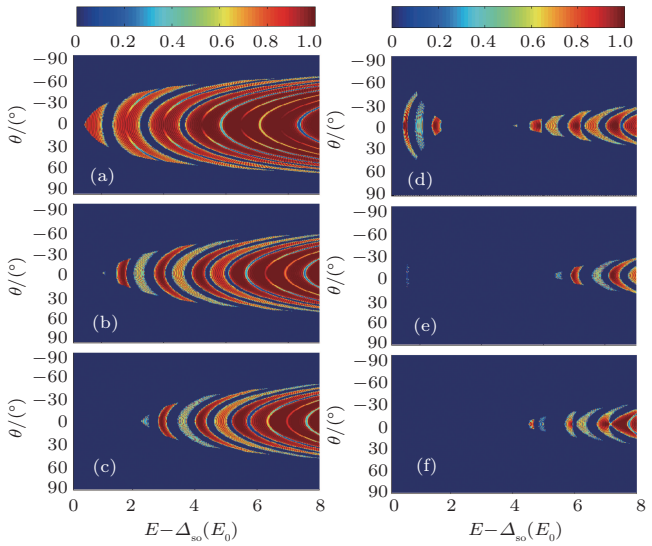



**Fig. 3.** (color online) The same as Fig. 2 but for the antiparallel configuration. The number of FM stripes is $N = 40$.

However, in the P configuration case $A_y(-x) = A_y(x)$, $\Delta_z(-x) = \Delta_z(x)$, $V(-x) = V(x)$, $H'_{\eta,\sigma}(-k_y) \neq H^*_{\eta,\sigma}(k_y)$, obviously this symmetry is broken, as shown in Fig. 2. For the case $\Delta_z \neq 0$ and $U_0 = 0$ of AP configuration, $E < \sqrt{B^2 + (\Delta_z - \eta\sigma\Delta_{so})^2}$ is the low-energy transmission-forbidden region arising from the evanescent modes in the superlattice region. For the case $\Delta_z = \Delta_{so}$ and $U_0 \neq 0$, the energy transmission-forbidden region becomes $U_0 - B < E < U_0 + B$ for $\eta\sigma = 1$ states, while $U_0 - \sqrt{B^2 + 4\Delta_{so}^2} < E < U_0 + \sqrt{B^2 + 4\Delta_{so}^2}$ for $\eta\sigma = -1$ states. Obviously, the forbidden region of $\eta\sigma = -1$ states is wider than that of $\eta\sigma = 1$, and thus there are energy ranges where only $\eta\sigma = 1$ states are transmitted [Comparing Fig. 3(b) with Fig. 3(c) and Fig. 3(d) with Fig. 3(e) ]. In comparison with the case of the P configuration, the transmission is strongly suppressed for both large negative and large positive incident angles in the AP case, and electrons tunnel through the periodic array of magnetic barriers more difficultly than that for the P configuration. This because some propagating modes in the normal regions cannot tunnel through the region IV of the AP configuration, while which can always transmit in the barrier region with P configuration.

Finally, we focus on the conductance ($G$) and the TMR. TMR usually has two definitions,[44,45] we adopt one of the definitions by

$$\mathrm{TMR} = \frac{G_P - G_{AP}}{G_P}, \tag{14}$$

where the subscript P (AP) denotes parallel (antiparallel) configuration, and $G_P$ ($G_{AP}$) is the total charge conductance for the P (AP) configuration. The total charge conductance is obtained by summing Eq. (13) over $\eta$ and $\sigma$. The other definition of TMR has $G_{AP}$ in the denominator. We choose this definition because in our case, $G_{AP}$ vanishes in some energy ranges.

We show the behavior of the conductances and TMR as a function of Fermi energy in Fig. 4. When both local gate voltage and external electric field are applied to FM stripes, the transmission is suppressed in the band gap of $U_0 - |\Delta_z - \eta\sigma\Delta_{so}| < E_F < U_0 + |\Delta_z - \eta\sigma\Delta_{so}|$ for $\eta\sigma = \pm 1$ states. Obviously, the $\eta\sigma = -1$ states experience a larger gap than the $\eta\sigma = 1$ states. Therefore, both $\eta\sigma = 1$ and $\eta\sigma = -1$ states are suppressed in the energy range of $U_0 - |\Delta_z - \Delta_{so}| < E_F < U_0 + |\Delta_z - \Delta_{so}|$ for P/AP configuration. This strong suppression of transmission leads to the vanishing of both $G_{AP}$ and $G_P$, so the TMR takes an indeterminate form in this energy regime. Therefore, in order to avoid such a case, we need to apply an external electric field $\Delta_z = \Delta_{so}$ to magnetic barrier regions. In Fig. 4, the conductance $G_P$ [see the black dot-dashed lines], $G_{AP}$ [see the blue dashed lines] and tunneling magnetoresistance ratio TMR [see the red solid lines] are plotted as a function of the Fermi energy for different heights of the electric and magnetic barriers. We can see that the conductances and TMR exhibit significant oscillations for both P and AP configurations. Obviously, the position of the conductance peaks and valleys for the Fermi energies correspond to the transmission peaks and valleys. The TMR also shows many peaks which are found for the Fermi energies corresponding to the valleys of $G_{AP}$. For the AP magnetization configuration, the transmission of electrons is drastically suppressed for all incident angles in an energy interval around the electrostatic potential. But away from this transmission suppressed region, $G_{AP}$ essentially increases with the Fermi energy. From the red solid curve in this figure, we can see that there is an energy range where the TMR reaches its maximum positive value 100% in the vicinity of $E_F = U_0$. Obviously, the position of this range can be changed by potential barrier height. Moreover, we find that the 100% TMR range widen with the increase of magnetic field. Here is the reason: when $E_F$ lies in the full transmission gap $[U_0 - B, U_0 + B]$, the conductance $G_{AP}$ is zero while the conductance $G_P$ can be large. Obviously this gap can be adjusted by $U_0$ and $B$. Furthermore, as we can see from Fig. 4, the curve of $G_{AP}$ is lower than that of $G_P$ at almost all energy region. However, we can observe the appearance negative TMR in Fig. 4(c) at the low-energy regime. Such negative values arises from the charge types of quasiparticles tunneling through the magnetic barriers reverse their

signs for the AP configuration.[45] The negative TMR disappears when the Fermi energy is large.

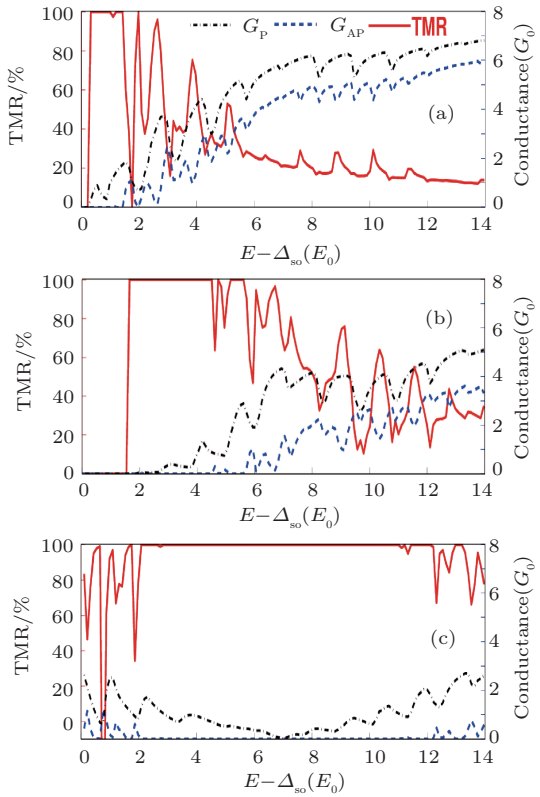



**Fig. 4.** (color online) The tunneling conductance $G_P$ (the black dot-dashed curves), $G_{AP}$ (the blue dashed curves) and tunneling magnetoresistance ratio TMR (the red solid curve) as a function of the Fermi energy for $\Delta_z = \Delta_{so}$, (a) $B = 1$, $U_0 = 1$; (b) $B = 4$, $U_0 = 1$; (c) $B = 4$, $U_0 = 8$. The number of FM stripes is $N = 40$.

## 4. Summary

In summary, we have investigated theoretically the quantum tunneling processes through a periodic array of magnetic and electric barriers on silicene sheet. Regardless of the magnetic field, whenever the $\Delta_z \neq 0$, there is an incident energy range where $\eta\sigma = 1$ states are transmitted, while $\eta\sigma = -1$ states are not. This energy range can be controlled by the electric gate voltage applied in the same region as the magnetic barriers. For the P magnetization configuration, the transmission is asymmetric with respect to the incident angle $\theta$. When the electric barrier height equals the magnetic barrier, electrons can always transmit via propagating states in the superlattice region with a large negative incident angle $\theta$ closing to $-90^\circ$ for $\eta\sigma = 1$ states except the suppressed low-energy regime. But for the AP configuration, the transmission is symmetric about $\theta$ and there is no such transmission channel because of the opposite vector potentials in barrier regions. Owing to the difference between P and AP configurations, the TMR can reach to 100% in a certain Fermi energy interval around the electrostatic potential. This interval can widen with the increase of magnetic field and be changed by the electric potential barrier. Our findings may be useful for spin-tronic and valley-tronic applications based on silicene and have certain practical significance in silicene-based magnetoresistance device.

## References


[1] Takeda K and Shiraishi K 1994 *Phys. Rev. B* **50** 14916
[2] Novoselov K S, Geim A K, Morozov S V, Jiang D, Zhang Y, Dubonos S V, Grigorieva I V and Firsov A A 2004 *Science* **306** 666
[3] Lalmi B, Oughaddou H, Enriquez H, Kara A, Vizzini S, Ealet B and Aufray B 2010 *Appl. Phys. Lett.* **97** 223109
[4] Vogt P, Padova P D, Quaresima C, Avila J and Frantzeskakis E 2012 *Phys. Rev. Lett.* **108** 155501
[5] Liu C C, Feng W and Yao Y 2011 *Phys. Rev. Lett.* **107** 076802
[6] Liu C C, Jiang H and Yao Y 2011 *Phys. Rev. B* **84** 195430
[7] Ezawa M 2012 *Phys. Rev. Lett.* **109** 055502
[8] Ezawa M 2012 *New J. Phys.* **14** 033003
[9] Yokoyama T 2013 *Phys. Rev. B* **87** 241409
[10] Soodchomshom B 2014 *J. Appl. Phys.* **115** 023706
[11] Wang R, Xu M S and Pi X D 2015 *Chin. Phys. B* **24** 086807
[12] Wang Y Y, Quhe R G, Yu D P and Lü J 2015 *Chin. Phys. B* **24** 087201
[13] Yao Y, Ye F, Qi X L, Zhang S C and Fang Z 2007 *Phys. Rev. B* **75** 041401(R)
[14] Drummond N D, Zólyomi V and Fal'ko V I 2012 *Phys. Rev. B* **85** 075423
[15] Tahir M, Manchon A, Sabeeh K and Schwingenschlögl U 2013 *Appl. Phys. Lett.* **102** 162412
[16] Kim Y, Choi K, and Ihm J 2014 *Phys. Rev. B* **89** 085429
[17] Ezawa M 2013 *Phys. Rev. Lett.* **110** 026603
[18] Kaloni T P, Singh N and Schwingenschló gl U 2014 *Phys. Rev. B* **89** 035409
[19] Pan H, Li Z, Liu C C, Zhu G, Qiao Z and Yao Y 2014 *Phys. Rev. Lett.* **112** 106802
[20] Bahram S and Mohsen Y 2017 *Chin. Phys. B* **26** 017203
[21] Tabert C J and Nicol E J 2013 *Phys. Rev. Lett.* **110** 197402
[22] Tahir M and Schwingenschló gl U 2013 *Sci. Rep.* **3** 1075
[23] Shakouri K, Vasilopoulos P, Vargiamidis V and Peeters F M 2014 *Phys. Rev. B* **90** 125444
[24] Cerchez M, Hugger S and Heinzel T 2007 *Phys. Rev. B* **75** 035341
[25] Hong J, Joo S, Kim T S, Rhie K, Kim K H, Kim S U, Lee B C and Shin K H 2007 *Appl. Phys. Lett.* **90** 023510
[26] Matulis A and Peeters F M 1994 *Phys. Rev. Lett.* **72** 1518
[27] Martino A D, Dell'Anna L and Egger R 2007 *Phys. Rev. Lett.* **98** 066802
[28] Dell'Anna L and Martino A D 2009 *Phys. Rev. B* **79** 045420
[29] Zhai F and Chang K 2008 *Phys. Rev. B* **77** 113409
[30] Wu Z, Peeters F M and Chang K 2011 *Appl. Phys. Lett.* **98** 162101
[31] Liu Y, Zhou X, Shao H, Zhou M and Zhou G 2014 *Physica B* **445** 81
[32] Wu X Q and Meng H 2015 *J. Appl. Phys.* **117** 203903
[33] Zhang Q, Chan K S and Long M 2016 *J. Phys.: Condens. Matter* **28** 055301
[34] Masir M R, Vasilopoulos P and Peeters F M 2010 *J. Phys.: Condens. Matter* **22** 465302
[35] Wang H, Chen X, Zhou X, Zhang L and Zhou G 2012 *Physica B* **407** 3664
[36] Moldovan D, Masir M R, Covaci L and Peeters F M 2012 *Phys. Rev. B* **86** 115431
[37] Xu H 1994 *Phys. Rev. B* **50** 8469
[38] Xu H 1995 *Phys. Rev. B* **52** 5803
[39] Ko D Y K and Inkson J C 1988 *Phys. Rev. B* **38** 9945
[40] Zhou J, Cheng S, You W L and Jiang H 2016 *Sci. Rep.* **6** 23211
[41] Tsai W F, Huang C Y, Chang T R, Lin H, Jeng H T and Bansil A 2013 *Nat. Commun.* **4** 1500
[42] Zhang Y Y, Tsai W F, Chang K, An X T, Zhang G P, Xie X C and Li S S 2013 *Phys. Rev. B* **88** 125431
[43] Bü ttiker M, Imry Y, Landauer R and Pinhas S 1985 *Phys. Rev. B* **31** 6207
[44] Yang X D, Wang R Z, Guo Y, Yang W, Yu D B, Wang B and Yan H 2004 *Phys. Rev. B* **70** 115303
[45] Saxena R, Saha A and Rao S 2015 *Phys. Rev. B* **92** 245412